Current Journal of Applied Science and Technology

39(3): 34-46, 2020; Article no.CJAST.53898
ISSN: 2457-1024
(Past name: British Journal of Applied Science & Technology, Past ISSN: 2231-0843, NLM ID: 101664541)

Low-cycle Fatigue Behavior and Constitutive Relations for a Ferritic Stainless Steel at Elevated Temperatures

S. M. Humayun Kabir[1*] and Tae-In Yeo[2]

[1]Department of Mechanical Engineering, Chittagong University of Engineering and Technology, Chittagong-4349, Bangladesh.
[2]School of Mechanical and Automotive Engineering, University of Ulsan, P.O.Box 18, Ulsan 680-749, Republic of Korea.

Authors' contributions

This work was carried out in collaboration between both authors. Both authors read and approved the final manuscript.

Article Information

DOI: 10.9734/CJAST/2020/v39i330512
Editor(s):
(1) Dr. Grzegorz Golanski, Institute of Materials Engineering, Czestochowa University of Technology, Poland.
Reviewers:
(1) Abeer Adel Salih, National University of Malaysia, Malaysia.
(2) Shashidhar K. Kudari, CVR College of Engineering, India.
Complete Peer review History: http://www.sdiarticle4.com/review-history/53898

Original Research Article

Received 03 December 2019
Accepted 10 February 2020
Published 12 March 2020

ABSTRACT

In this paper, the tensile and strain-controlled cyclic deformation behavior of a ferritic stainless steel which is developed for the exhaust manifold of automobiles is evaluated experimentally at different temperatures. The effect of temperature on monotonic tensile responses such as yield strength and ultimate tensile strength and the effect of temperature and strain amplitude on the evolution of peak stress are assessed. The objective of this study is also to reveal the mixed mode of cyclic hardening–softening behavior of the ferritic stainless steel under strain-controlled fatigue test conditions. A parameter, critical accumulated plastic strain, is introduced to the constitutive equations for the material for describing the hardening - softening responses. The nonlinear constitutive equations for describing the cyclic responses are implemented into Finite Element code using determined parameters for obtaining numerical simulation. The stabilized hysteretic responses obtained from experiment and predicted from numerical simulation are compared and found to be realistic.

**Corresponding author: E-mail: dalimuou@yahoo.com;*

Keywords: Ferritic stainless steel; monotonic response; cyclic hardening/softening; accumulated plastic strain; finite element code.

NOMENCLATURES

$\boldsymbol{\sigma}$: *Stress tensor*
σ_y : *Size of the yield surface*
σ_{y0} : *Initial size of the surface*
α : *Back stress tensor*
α' : *Deviatoric part of back stress tensor*
$\Delta\sigma/2$: *Stress amplitude*
$\Delta\varepsilon/2$: *Strain amplitude*
$\boldsymbol{\varepsilon_p}$: *Plastic strain tensor*
$\boldsymbol{\varepsilon_e}$: *Elastic strain tensor*
$d\boldsymbol{\varepsilon_p}$: *Increment of plastic strain tensor*
$\boldsymbol{\sigma}_{\text{dev}}$: *Deviatoric stress tensor*
${}^{n+1}\boldsymbol{\sigma}^{\text{tr}'}$: *Deviatoric Trial Stress*
G , K : *Lame constants*
K_b : *Elastic bulk modulus*
$\boldsymbol{I}$: *Second order identity tensor*
$\boldsymbol{l}$: *Fourth order identity tensor*
r : *Isotropic hardening function*
r_1, r_2 : *Isotropic hardening functions*
b_1 : *The rate of saturation of* r_1
b_2 : *The rate of saturation of* r_2
Q_1 : *Saturated value of* r_1
Q_2 : *Saturated value of* r_2
C, γ : *Kinematic hardening parameters*
f : *Yield function*
Δp : *Increment of accumulated plastic strain*
p_{cr} : *Critical accumulated plastic strain*

1. INTRODUCTION

Many engineering components experience cyclic loadings under isothermal and anisothermal conditions during their service life, such as exhaust manifold systems of automobile, wheels in railroad industry, pressure vessels in chemical or power plants, and so on. Now-a-days, increased operating temperature is very common for improved performance in high-temperature structure. Consequently, the properties, such as light weight, high corrosion resistance, and fairly high thermal fatigue resistance are of greater importance in selection of material for high temperature-structure such as in exhaust manifold systems of automotives. So the material parameters and mechanical properties of structural steels in elasto-plastic cyclic behavior at elevated temperature have gained interests in many studies during recent years to replace cast iron, the traditional material for these applications [1-5]. For years, various theoretical constitutive models based on continuum mechanics have been developed for describing the material nonlinearities and allowing accurate modeling of hardening/softening responses under cyclic loading conditions [6-10]. And, characterization of material parameters are important research concerning accurate presentation of inelastic responses of engineering components.

Even though austenitic stainless steel has better strength at elevated temperatures than ferritic stainless steel, the use of ferritic stainless steel has also been increased due to its excellent corrosion resistance, moderate thermal fatigue resistance, and low prices. In this study, monotonic tensile and strain-controlled low cycle fatigue results are investigated on a ferritic stainless steel which is developed for the exhaust manifold used in exhausts system of automobiles. This study analyzes the influence of temperature and strain amplitude on monotonic and cyclic responses over a wide range of temperatures. Thereafter, a presentation of the temperature effect on tensile properties of the material, description of the mixed mode of cyclic hardening–softening behavior of the material under the fatigue test conditions, an introduction of critical accumulated plastic strain to the constitutive equations for describing the cyclic hardening - softening responses of the material, determination of material parameters of constitutive equations and a brief description of the simulation of the adopted constitutive equations utilizing the determined parameters, and comparison of analysis results with those of the experimental stabilized hysteresis loops at different temperatures are presented in subsequent sections.

2. MATERIALS AND EXPERIMENTAL RESULTS

In this study, tensile and strain-controlled low cycle fatigue data of a 400-series ferritic stainless steel designated as SS400-C over a wide range

of temperature is employed to examine the material responses. Nominal chemical compositions of the ferritic stainless steel are shown in Table 1. The ferritic stainless steel is developed for the exhaust manifold used in exhausts system of automobiles. A closed-loop servo-hydraulic test system with 10-ton capacity is used to conduct tensile and low-cycle fatigue tests. The specimens used in this study are fabricated with the required surface preparation in accordance with ASTM Standard E606-92. The shape and dimensions of polished specimens used in low cycle fatigue test under strain-controlled condition is shown in Fig. 1. To create a high-temperature environment, the specimen is heated using induction heating method where the measurement and control of temperature is accomplished by thermocouples. The experimental procedure at high-temperature consists of heating the specimen from room temperature to the testing temperature and holding at this temperature for 30 minute before starting the test. The tensile tests are carried out at a constant cross-head speed of 4.80 mm/min. The specimen temperature is made as uniform as possible by locating the induction coil on optimal locations with optimal number of turns which is found by several pre-experiments. In this measurement, the cross-head speed of 4.80 mm/min corresponds to apparent strain rate of 2×10^{-3} /s. Isothermal low-cycle fatigue tests are carried out under fully-reversed total strain-controlled procedure applying a triangular waveform with a constant strain rate of 2×10^{-3} /s. The low-cycle fatigue test are performed at different total strain amplitude ranging from $\Delta\varepsilon/2$ = 0.3% to $\Delta\varepsilon/2$ = 0.7% at different temperatures. The strain amplitudes and stress amplitudes are determined at stabilized loop of each specimen.

2.1 Monotonic Tensile Responses

The influence of temperature on yield strength and ultimate tensile strength (UTS) are examined which show that material strengths decrease with increasing temperature. It can be seen through Fig. 2 and Fig. 3 that in temperature region 200°C - 600°C, the reduction of yield strength and UTS are retarded or slightly decreased compared with other temperature regime. Fig. 4 demonstrates the serration [11] of tensile stress-strain curve of SS400-C where it is evident that serrated flow is well-defined in the temperature regime of 100°C - 600°C. Based on a recent study and survey [12] on the evidence of dynamic strain ageing (DSA) [13,14] in ferritic stainless steel, it is believed that plateau in the variation of yield strength and UTS and pronounced serrated flow demonstrated by the present material at intermediate temperature regime of 200°C - 600°C are the manifestations of DSA in terms of monotonic loading conditions. DSA has been explained in terms of the interaction between moving dislocations and diffusing solute atoms, which happens in a certain temperature range [12-14]. Hong and Lee [15] observed the similar phenomena of DSA for a carbon steel with different temperature range. DSA can be considered effective in strengthening steels when an anomaly appears in the flow stress vs temperature dependence. But DSA has deteriorating effect on fatigue life [12,16-19].

Table 1. Chemical composition of the SS400-C ferritic stainless steel (wt%)

C	Si	P	S	Cr	Mn	Mo	Nb
0.025	1.00	0.04	0.03	17.00	1.00	1.12	0.60

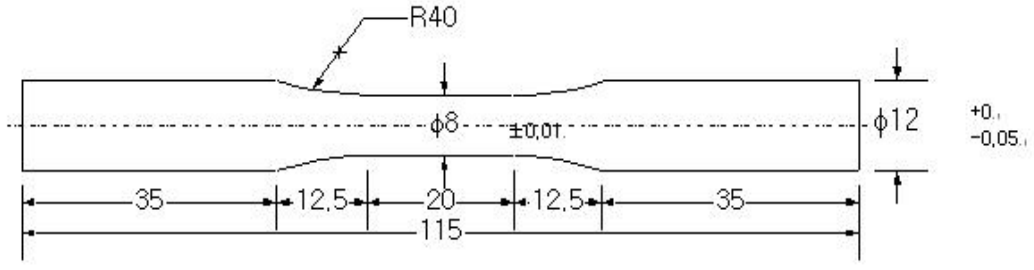

Fig. 1. Geometry of the low-cycle fatigue specimen, dimensions are in mm (fabricated with the required surface preparation in accordance with ASTM Standard E606-92)

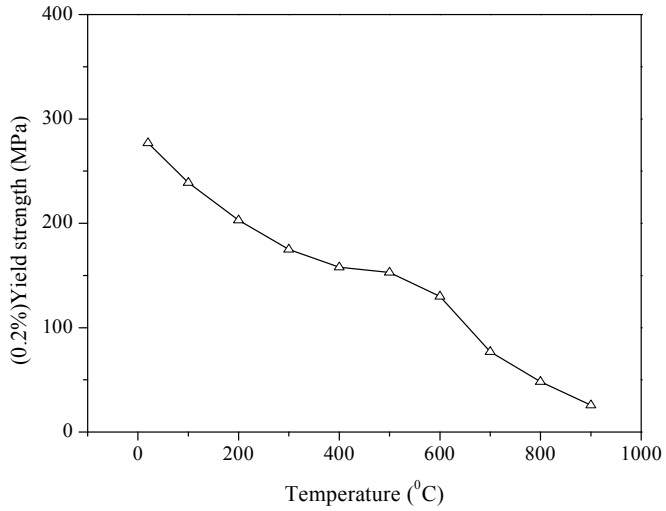

Fig. 2. The yield strength of SS400-C ferritic stainless steel depends on temperature

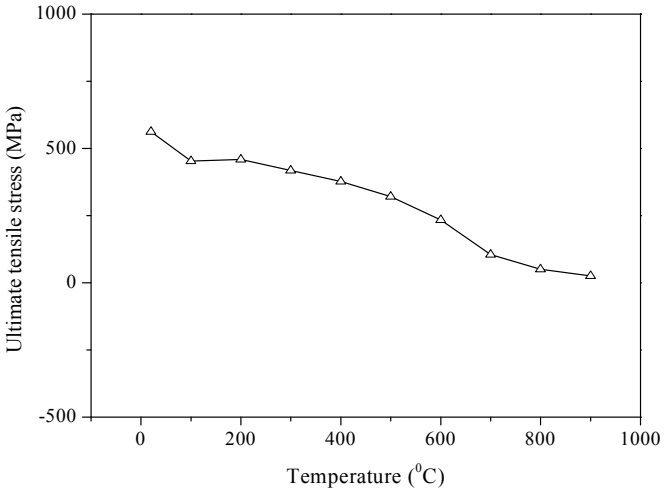

Fig. 3. The ultimate tensile strength of SS400-C ferritic stainless steel depends on temperature

2.2 Isothermal Cyclic Deformation Behavior and Peak Stress Evolution

Temperature and strain amplitude affect the cyclic deformation behavior of materials significantly. Fig. 5 and Fig. 6 are the typical representation of the influence of strain amplitude and temperature on the evolution of peak stress versus applied cycles for the material SS400-C. Fig. 5 depicts that the peak stresses increase with the increasing strain amplitude. These figures indicate that SS400-C exhibits initial cyclic hardening for nearly first 10 cycles followed by cyclic softening during most of the fatigue life for the temperature range RT ~ 300°C. Here, RT stands for room temperature. But at 500°C and 600°C, the cyclic hardening phenomena are dominant throughout the low cycle fatigue life. Different authors reported similar remarkable hardening in cyclic stress response of ferritic stainless steels [4,5,12]. This remarkable hardening is considered to be a DSA manifestation. The regime for dependence of marked cyclic hardening lies in the DSA regime of anomalous dependence of flow stress and dynamic strain hardening stress with temperature and serration regime of monotonic response. Kruml and Pola'k [20] and Pola'k et al. [21] noticed the similar mixed mode of Cyclic hardening–softening phenomena in case of X10CrAl24 and 446 ferritic stainless steels respectively. Cyclic softening in ferritic stainless steel was also found in other literatures [22-24]. An important feature of the cyclic straining of polycrystalline materials is the redistribution of the cyclic plastic strain and its localization. The

increase of dislocation density caused by strain cycling leads to decrease in dislocation mobility; hence hardening occurs usually.

Kruml and Pola'k [20] reported that high density of screw dislocations from several slip systems is produced within first few cycles, and no rearrangement to the spatial dislocation structures were found in the majority of grains when examined a ferritic stainless steel. It was also reported that the redistribution of the cyclic plastic strain and its localization is the source of cyclic softening at the later stage of life. Literatures [12,25,26] suggest that initial hardening could results from combination of formation of fine precipitates on dislocations during testing and DSA as a consequence of interaction between dislocations and solute atoms. Therefore, it is reasonable to be believed that the initial hardening of the present material could result from either individual or combined effects of (i) mutual interaction among dislocations and (ii) formation of fine precipitates on dislocations during testing, and (iii) DSA. And, cyclic softening can be related to the localization of the cyclic plastic strain into the bands of intensive cyclic slip [21]. The typical stabilized hysteresis loops at different strain amplitude ($\Delta\varepsilon/2$ = 0.3% ~ $\Delta\varepsilon/2$ = 0.7%) are translated to the lower peak in Fig. 7 for the temperature of 200°C. Fig. 7 indicates that magnitude of the stabilized stress increases with the increase of strain amplitude for a particular temperature.

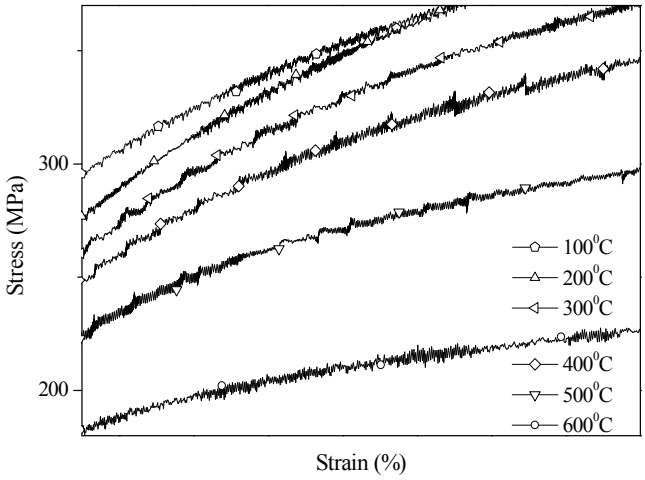

Fig. 4. The stress-strain curve of SS400-C ferritic stainless steel under temperature range of 100°C - 600°C

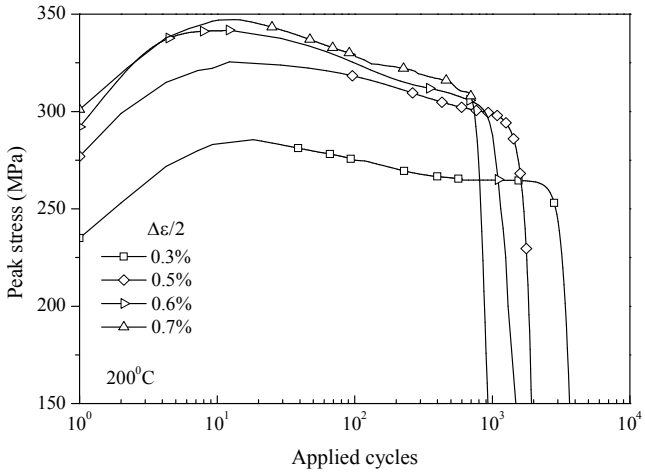

Fig. 5. The influence of strain amplitude on the evolution of peak stress of the ferritic stainless steel at 200°C

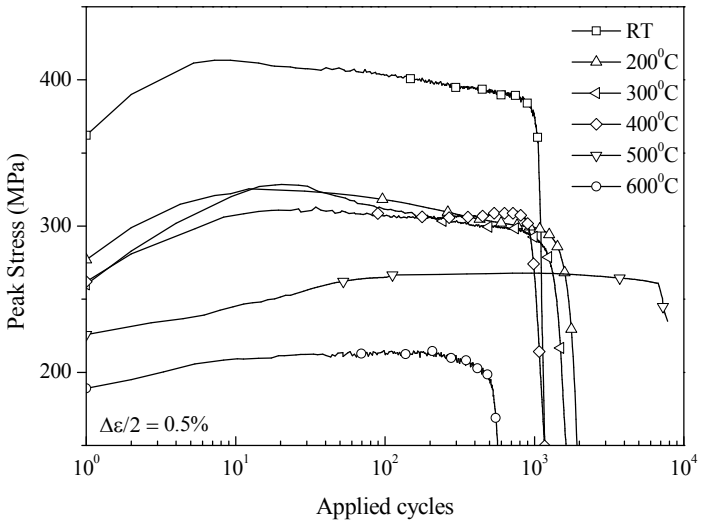

Fig. 6. The influence of temperatures on evolution of peak stress of the ferritic stainless steel at $\Delta\varepsilon/2 = 0.5\ \%$

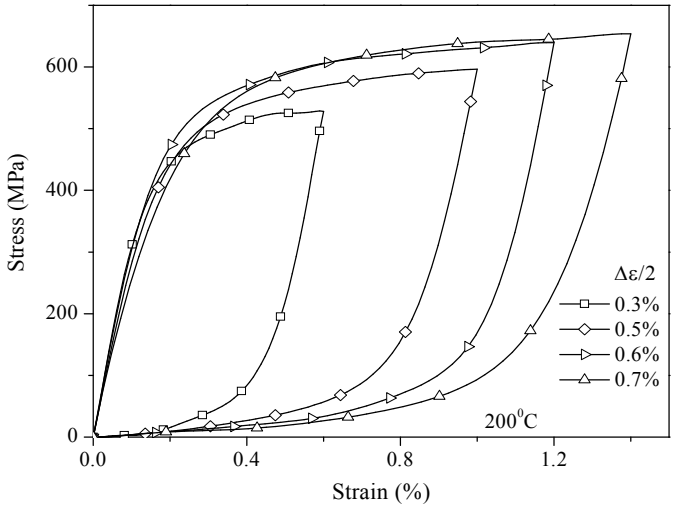

Fig. 7. Stabilized hysteresis loops of the SS400-C ferritic stainless steel adjusted to the lower peak

3. CONSTITUTIVE EQUATIONS

For stainless steel, it is well recognized that materials undergo through cyclic hardening or cyclic softening. Within an individual cycle, kinematic hardening is the dominant hardening process, but over a large number of cycles the materials also hardens or softens isotropically such that peak stress and strain in a hysteresis loop increase or decrease from one cycle to the next until saturation is achieved [27]. The amount of expansion or contraction of yield surface is often taken to be a function of accumulated plastic strain p [27],

$$p = \int dp \tag{1}$$

with the increment in accumulated plastic strain $dp = \sqrt{(2/3)(d\boldsymbol{\varepsilon}_p : d\boldsymbol{\varepsilon}_p)}$, where the operator ':' represents double contraction.

The rate independent plasticity models considered in this study have the following common features:

i) von-Mises yield criterion (yield surface): The elastic domain is defined by,

$$f(\boldsymbol{\sigma}-\alpha)=\sqrt{\frac{3}{2}}\left|\boldsymbol{\tau}_{\mathrm{dev}}\right|-\sigma_y(p)=0 \quad (2)$$

With

$$\boldsymbol{\tau}_{\mathrm{dev}}=\boldsymbol{\sigma}_{\mathrm{dev}}-\alpha' \text{ and } \left|\boldsymbol{\tau}_{\mathrm{dev}}\right|=\sqrt{\boldsymbol{\tau}_{\mathrm{dev}}:\boldsymbol{\tau}_{\mathrm{dev}}} \quad (3)$$

$$\boldsymbol{\sigma}_{\mathrm{dev}}=2G\boldsymbol{I}_{dev}:\boldsymbol{\varepsilon}_e \quad (4)$$

$$\boldsymbol{I}_{dev}=\boldsymbol{I}-(1/3)\boldsymbol{I}\otimes\boldsymbol{I} \quad (5)$$

ii) Size of the surface,

$$\sigma_y(p)=\sigma_{y0}+r(p) \quad (6)$$

iii) The evolution of isotropic variable [8,10],

$$dr=b(Q-r)dp \quad (7)$$

iv) The evolution of kinematic hardening variable [6],

$$d\alpha'=\frac{2}{3}Cd\boldsymbol{\varepsilon}_p-\gamma\alpha' dp \quad (8)$$

where, $\boldsymbol{\sigma}_{\mathrm{dev}}$ is the deviatoric part of stress tensor $\boldsymbol{\sigma}$, α is the current center of the yield surface in total stress space, α' is the current center of the yield surface in deviatoric stress space, f is the yield function, σ_y is the size of the yield surface which takes into account the initial yield size σ_{y0} and isotropic function r, σ_{y0} is the initial size of the surface with $r(0)=0$, Q is the stabilized value of r, constant b controls the pace of the isotropic hardening, and C and γ are material constants regarding kinematic hardening.

For the material SS400-C, Fig. 8 shows that stress increases with respect to cycles up to the stabilization at 400°C but stress increases for a first few cycles and decreases up to the stabilization state for other temperatures. Due to mixed mode of evolution of stress with respect to cycles, using Eq.(7) two isotropic variables with a parameter critical accumulated plastic strain p_{cr} is introduced in this study for the evolution of isotropic variable in the following manner,

$$r=Q_1(1-e^{-b_1 p})-H(p-p_{cr})[Q_2(1-e^{-b_2(p-p_{cr})})] \quad (9)$$

with the following two criteria

$$\begin{aligned} &if\ \ p_{cr}\neq 0\ \ and\ \ (p-p_{cr})>0\ \ then\ H(\cdot)=1 \\ &\qquad\qquad (p-p_{cr})<0\ \ then\ H(\cdot)=0 \end{aligned} \quad (10)$$

and

$$if\ \ p_{cr}=0\ \ and\ \ (p-p_{cr})>0\ \ then\ H(\cdot)=-1 \quad (11)$$

where, in Eq.(9), H(.) is a Heaviside Step Function, and the first isotropic variable r_1 is,

$$r_1=Q_1(1-e^{-b_1 p}) \quad (12)$$

and second isotropic variable r_2 is,

$$r_2=Q_2(1-e^{-b_2(p-p_{cr})}) \quad (13)$$

and p_{cr} is the critical accumulated plastic strain above which second isotropic variable works. Q_1 and Q_2 represent the asymptotic values of the isotropic variables r_1 and r_2 respectively. b_1 and b_2 represent the stabilization curve steepness for the isotropic variables r_1 and r_2 respectively. First isotropic variable represents the cyclic hardening and second isotropic variables demonstrates the cyclic hardening or softening depending upon the above two criteria. Therefore, p_{cr} controls the mode of cyclic response which is a function of temperature for particular strain amplitude.

4. ANALYSIS

In this section, extraction of material parameters and how the constitutive equations are implemented into finite element simulation are stated in a brief. The simulation results are also compared with that of the experiment.

4.1 Material Parameters

Considering that low cycle fatigue failure occurs usually after several hundreds of load cycles, the parameters are calibrated using the stabilized loops. Identifying the parameters to find the stabilized hysteresis loop in an elasto-plastic steel behavior, is an important step concerning low cycle fatigue life studies. The plastic

parameters are determined with the available strain-controlled cyclic tests data at isothermal condition. Correlating two constitutive models [28] in terms of their parameters, determination of hardening parameters is done systematically and efficiently for structural steels which either cyclically harden or soften. In this approach [28], the critical accumulated plastic strain p_{cr} is introduced which controls the mode of cyclic responses depicted in Fig. 5 and Fig. 8. The critical accumulated plastic strain is calculated easily first at $\Delta\varepsilon/2 = 0.7\,\%$ for different temperature from Fig. 7. Then, isotropic parameters Q_1, Q_2, b_1, and b_2 are determined. On the determination of isotropic parameters, isotropic parameters Q_1 and b_1 of first isotropic variable are determined with a nonlinear regression procedure and then isotropic parameters Q_2 and b_2 of second isotropic are determined minimizing the strain-energy density [28]. Utilizing the concept of stabilized elastic limit [28], the Young's modulus is derived directly from the linear part of the stabilized hysteresis loop (Fig. 7) which is denoted here as E^*. The Young's modulus from the first tensile curve differs by 10% ~ 12% than that of at stabilized loops. The experimental curve of stress versus plastic strain is obtained directly from the stabilized loop from which the experimental kinematic hardening (α) is extracted. Finally, utilizing stabilized hysteresis loop data with the built-in calibration procedure of the ABAQUS code, C and γ of kinematic hardening variable are determined. Detail procedure for determining the material parameters can be found elsewhere [28]. The determined parameters for different materials are listed in Table 2 and Table 3.

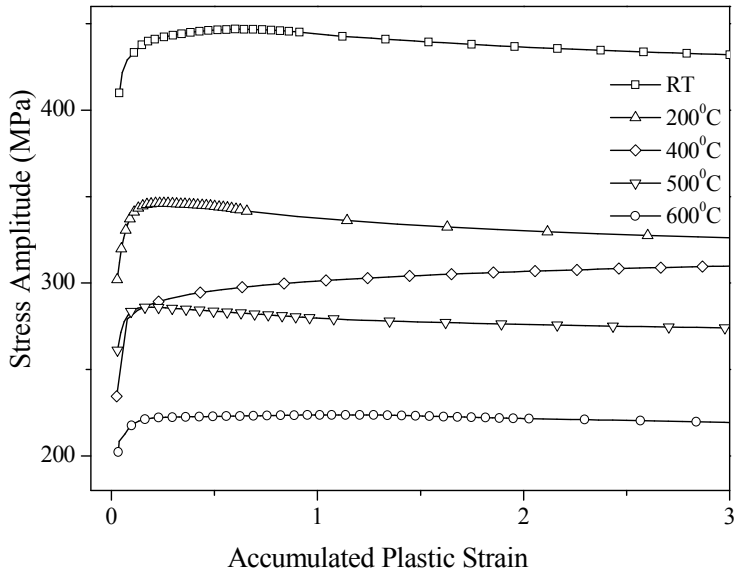

Fig. 8. Experimental $\Delta\sigma/2 - p$ curves of the SS400-C ferritic stainless steel at different temperatures

Table 2. Isotropic parameters with p_{cr} at $\Delta\varepsilon/2 = 0.7\,\%$

Temp. °C	E^* (GPa)	σ_{y0} (MPa)	Q_1 (MPa)	Q_2 (MPa)	b_1	b_2	p_{cr}
RT	269	219	37	21	9.4	0.50	0.631
200	206	189	47	30	17	0.51	0.308
400	144	134	53	22	16	1.10	0.000

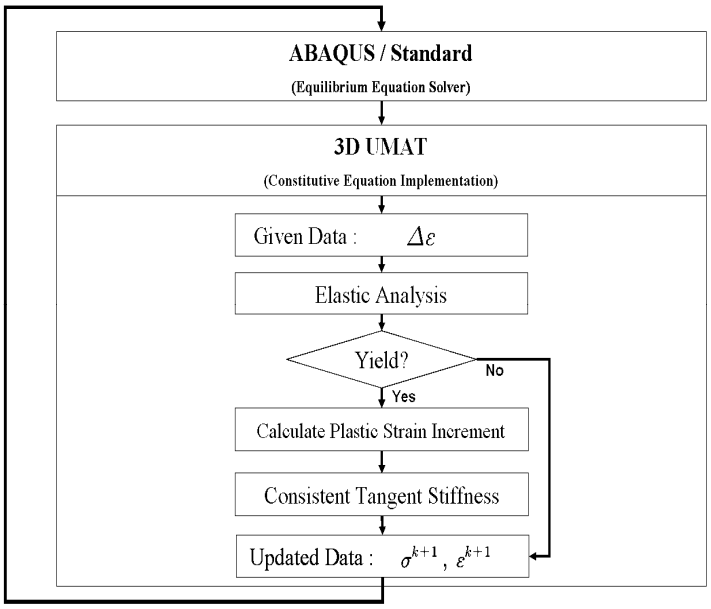

Fig. 9. Incorporation of UMAT with ABAQUS

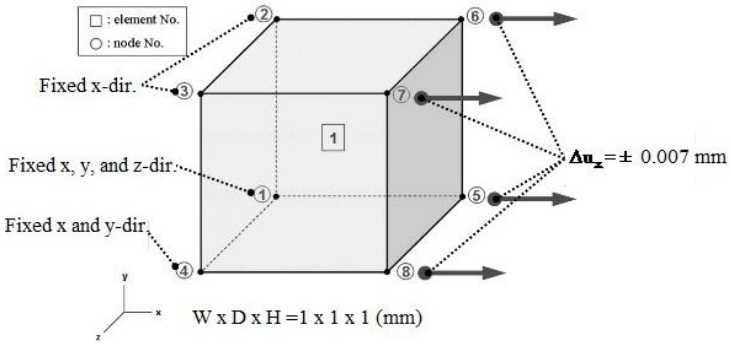

Fig. 10. Boundary conditions for finite element analysis

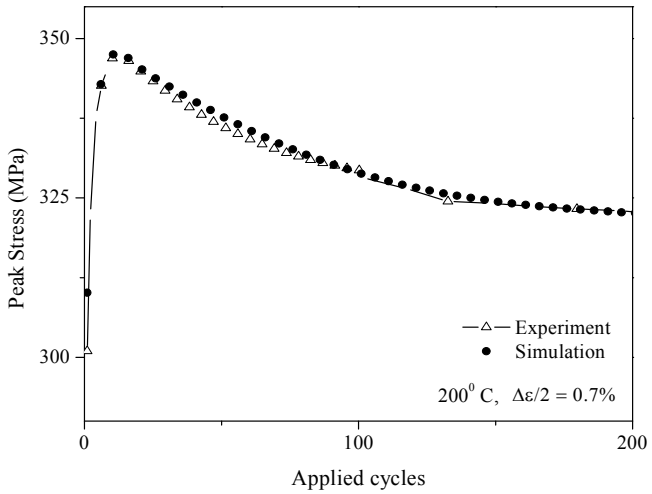

Fig. 11. Comparison of simulation results of typical evolution of peak stress with that of experimental responses

Table 3. Kinematic hardening parameters at $\Delta\varepsilon/2 = 0.7\ \%$

Temp. °C	C (MPa)	γ
RT	140788.00	869.53
200	54667.97	599.41
400	67297.59	736.43

4.2 Numerical Simulation and Results

The implicit Backward Euler algorithm is favored by many researchers for large increments because of its stability and accuracy characteristics. An algorithm for implementation of the Combined Non-linear hardening rule has been proposed in [29] and modified in [30], whereby discretized rate equation reduced to one-dimensional problem. For numerical simulation, we apply the implicit integration scheme in strain-driven approach in a similar fashion described in [30] and the resulting discretized equations for the non-linear constitutive equations mentioned in section 3 are summarized as follows,

$$^{n+1}f = \sqrt{\frac{3}{2}}\left|{}^{n+1}\boldsymbol{\tau}^{\mathrm{tr}}_{\mathrm{dev}}\right| - (3G + {}^{n+1}\Phi C)\Delta p - {}^{n+1}r(\Delta p) - \sigma_{y0} = 0 \tag{14}$$

with

$$^{n+1}\boldsymbol{\tau}^{\mathrm{tr}}_{\mathrm{dev}} = {}^{n+1}\boldsymbol{\sigma}^{\mathrm{tr}'} - {}^{n+1}\Phi\ {}^{n}\alpha' \tag{15}$$

$$^{n+1}\Phi = 1/(1+\gamma\,\Delta p) \tag{16}$$

$$^{n+1}\boldsymbol{\sigma}^{\mathrm{tr}}_{\mathrm{dev}} = 2G({}^{n}\boldsymbol{\varepsilon}_e + \Delta\boldsymbol{\varepsilon}) + (K - K_b)\boldsymbol{I}({}^{n}\boldsymbol{\varepsilon}_e + \Delta\boldsymbol{\varepsilon}) : \boldsymbol{I} \tag{17}$$

This system of equations in the implicit scheme is termed here as a local problem where, the index $n+1$ represents the current time step. If the material is in the plastic region then the unknown variable Δp is to be solved out. After the local problem has been solved, the stress, accumulated plastic strain, and other variables are updated and a new strain increment is taken. In Eq. (11), isotropic variable r is evolved according to the Eq. (9) depending upon the criteria associated with the critical accumulated plastic strain p_{cr}.

The nonlinear constitutive equations are implemented into Finite Element (FE) code through ABAQUS by means of a UMAT (User subroutine to define a Material's mechanical behavior) subroutine. The incorporation of UMAT in Finite Element software works as in Fig. 8. To obtain the good convergence, we provide a consistent tangent stiffness matrix to ABAQUS through UMAT subroutine. This consistent tangent stiffness matrix provides the information about the material behavior. We combine the Bisection method with Newton-Rhapson iteration for better convergence in iterative procedure. In FE simulation, only one finite element, in the middle of the sample, is submitted to an imposed strain $\Delta\varepsilon/2 = \pm 0.007$ and subsequently analysis is carried out. The proper boundary condition imposed on the element is described graphically in Fig. 10.

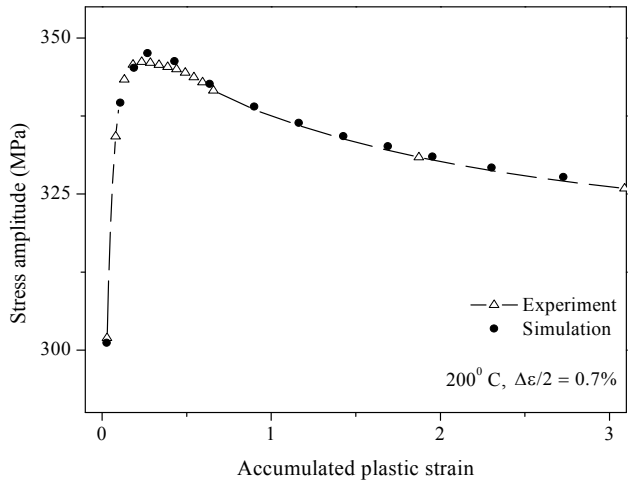

Fig. 12. Comparison between experimental responses and simulation results of a $\Delta\sigma/2 - p$ curve

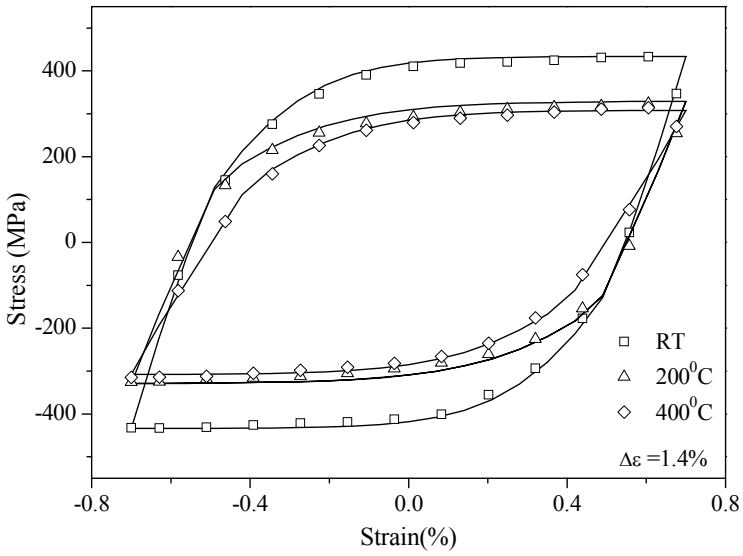

Fig. 13. Comparisons of stabilized hysteresis loops for the ferritic stainless steel (Solid Lines: Simulation results, Symbols: Experimental data)

The simulations of typical evolution of peak stress with respect to applied cycles and variation of stress amplitude with respect to accumulated plastic strain ($\Delta\sigma/2-p$) are presented and compared with that of experimental responses in Fig. 11 and Fig. 12 respectively. In both cases, good correlation is obtained between the simulated responses and the experimental observations. The experimental results of stabilized hysteresis loops together with UMAT results for the material considered are shown in Fig. 13. The prediction of stabilized loops coincides well with the experimental results. Comparisons reveal that incorporation of critical accumulated plastic strain are said to be reasonable to represent mixed mode of evolution of stress (hardening and softening) for the material considered.

5. CONCLUSION

Inelastic responses of a ferritic stainless steel are carefully experimentally studied under tensile monotonic and low cycle fatigue tests. Several tests have been performed to derive the basic data. The obtained results are as follows:

a. Tests results have shown a strong influence of temperature and strain amplitude on monotonic responses as well as on low cycle responses.
b. Under monotonic tensile test, anomalous dependence of flow stress with temperature and serrations in stress-strain curves are believed to be manifestations of DSA.
c. The material displays mixed mode of hardening and softening behavior at different temperatures when the material is subjected to cyclic loadings and the peak stresses increase with the increasing strain amplitude. An attempt is made to introduce the critical accumulated plastic strain above which second isotropic variable works for describing mixed mode of cyclic responses.
d. For comparison purpose, constitutive equations are implemented into finite element simulation considering mixed mode of cyclic hardening-softening. It is noteworthy that the simulation results with determined material parameters predict well the experimental stabilized loops at different temperatures.

ACKNOWLEDGEMENT

The authors express their thanks to SEJONG INDUSTRIAL CO. LTD., Republic of Korea for the support in acquiring of the material data.

COMPETING INTERESTS

Authors have declared that no competing interests exist.

REFERENCES

1. Beddos J, Parr JG. Introduction to stainless steels. 3rd Edition, ASM Intl; 1998.
2. Li H, Nishimura A, Li Z, Nagasaka T, Muroga T. Low cycle fatigue behavior of JLF-1 steel at elevated temperatures. Fusion Eng. Des. 2006;81:241-245.
3. Vanaja J, Laha K, Sam S, Nandagopal M, Selvi SP, Mathew MD, Jayakumar T, Kumar ER. Influence of strain rate and temperature on tensile properties and flow behaviour of a reduced activation ferritic–martensitic steel. J. Nucl. Mater. 2012;424(1-3):116-122.
4. Lee KO, Yoon S, Lee SB, Kim BS. Low cycle fatigue behavior of 429EM ferritic steel at elevated temperatures. Key Eng. Mat. 2004;261-263:1135-1140.
5. Avalos M, Alvarez-Armas I, Armas AF. Dynamic strain aging effects on low-cycle fatigue of AISI 430F. Mater. Sci. Eng. A. 2009;513-514:1-7.
6. Armstrong PJ, Frederick CO. A mathematical representation of the multiaxial Bauschinger effect. G.E.G.B. Report RD/B/N. 1966;731-747.
7. Dafalias YF, Popov EP. Plastic internal variables formalism of cyclic plasticity. J. Appl. Mech. 1976;43:645-650.
8. Chaboche JL. Time-independent constitutive theories for cyclic plasticity. Int. J. Plasticity. 1986;2(2):149-188.
9. Chiang DY, Beck JL. A new class of distributed-element models for cyclic plasticity-I. Theory and applications. Int. J. Solids Struct. 1994;31:469-484.
10. Chaboche JL. A review of some plasticity and viscoplasticity constitutive theories. Int. J. Plasticity. 2008;24:1642–1693.
11. Rodriguez P. Serrated plastic flow. Bull. Mater. Sci. 1984;6(4):653-663.
12. Kabir SMH, Yeo T. Influence of temperature on a low-cycle fatigue behavior of a ferritic stainless steel. J. Mech. Sci. Technol. 2014;28(7):2595-2607.
13. Cottrell AH, Bilby BA. Dislocation theory of yielding and strain ageing of iron. Proc. Phys. Soc. A. XII. 1949;49-62.
14. Kubin LP, Estrin Y. Dynamic strain ageing and mechanical response of alloys. J. Phys. 1991;3(6):929-943.
15. Hong SG, Lee SB. Influence of strain rate on tensile and LCF properties of prior cold worked 316L stainless steel in dynamic strain aging regime. Fatigue Damage Materials: Experiment and Analysis, WIT Press. 2003;137-147.
16. Abdel-Raouf H, Plumtree A, Topper TH. Effects of temperature and deformation rate on cyclic strength and fracture of low carbon steel. ASTM STP. 1973;519:28-57.
17. Bressers J. High temperature alloys, their exploitable potential. J. B. Marriott, M. Merz, J. Nihoul, J. Ward, Editors, Elsevier Applied Science. 1987;385-410.
18. Srinivasan VS, Sandhya R, Valsan M, Rao KBS, Mannan SL, Sastry DH. The influence of dynamic strain ageing on stress response and strain-life relationship in low cycle fatigue of 316L(N) stainless steel. Scripta Mater. 1997;37(10):1593-1598.
19. Hong SG, Lee SB. The tensile and low-cycle fatigue behavior of cold worked 316L stainless steel: Influence of dynamic strain aging. Int. J. Fatigue. 2004;26:899-910.
20. Kruml T, Pola´k J. Fatigue softening of X10CrAl24 ferritic steel. Mater. Sci. Eng. A. 2001;319–321,564–568.
21. Pola´k J, Fardoun F, Degallaix S. Analysis of the hysteresis loop in stainless steels I. Austenitic and ferritic steels. Mater. Sci. Eng. A. 2001;297:144-153.
22. Pohl K, Mayr P, Macherauch E. Cyclic deformation behavior of a low carbon steel in the temperature range between room temperature and 850K. Int. J. Fracture. 1981;17:221-233.
23. Roven HJ, Nes E. Cyclic deformation of ferritic steel: I. Stress–strain response and structure evolution. Acta Metall. Mater. 1991;39:1719-1733.
24. Petersmeier T, Martin U, Eifler D, Oettel H. Cyclic fatigue loading and characterization of dislocation evolution in the ferritic steel X22CrMoV121. Int. J. Fatigue. 1998;20: 251-255.
25. Shankar V, Valsan M, Kannan R, Rao KBS, Mannan SL, Pathak SD. Low cycle fatigue behavior of a modified 9Cr-1 Mo Ferritic steel. ISRS on Material Science and Engineering, Chennai, India; 2004.
26. Nagesha A, Valsan M, Kannan R, Bhanu Sankara Rao K, Mannan SL. Influence of temperature on the low cycle fatigue behaviour of a modified 9Cr–1Mo ferritic steel, Int. J. Fatigue. 2002;24:1285-1293.
27. Dunne F, Petrinic N. Introduction to computational plasticity. Oxford University Press; 2005.

28. Kabir SMH, Yeo T. Characterization of unified material parameters in elasto-plastic continuum approach. Int. Rev. Mech. Eng. 2010;4(5):507-517.
29. Doghri I. Fully implicit integration and consistent tangent modulus in elasto-plasticity. Int. J. Num. Meth. Eng. 1993;36: 3915–3932.
30. Mahnken R. Improved implementation of an algorithm for nonlinear isotropic – kinematic hardening. Comm. Num. Meth. Eng. 1999;15:745-754.

© 2020 Kabir and Yeo; This is an Open Access article distributed under the terms of the Creative Commons Attribution License (http://creativecommons.org/licenses/by/4.0), which permits unrestricted use, distribution, and reproduction in any medium, provided the original work is properly cited.

Peer-review history:
The peer review history for this paper can be accessed here:
http://www.sdiarticle4.com/review-history/53898